Curvature Classification for Trains using Along-Track and Cross-Track Accelerometer and a Heading Rate Gyroscope

Boubeker Belabbas, Anja Grosch, Oliver Heirich, Andreas Lehner, and Thomas Strang
German Aerospace Center, Institute of Communications & Navigation, Oberpfaffenhofen, 82234 Wessling, Germany
mail: boubeker.belabbas@dlr.de

***Abstract*—Real time curvature classification is crucial for all train localization problems. A reliable method to detected the track taken by the train after a switch is necessary and essential for train collision avoidance systems. At a larger scale, this should be included in a global surveillance system. In this paper, we discuss three possible track curvature detection methods based on two accelerometers and one gyroscope. We define and analyze corresponding test statistics that determine the actual track curvature. Given system safety requirements, i.e., maximum allowable probabilities of false alert and miss-detection, we derive a minimum detectable curvature difference (MDCD) between two possible tracks and compare these values with standard curvatures used in Germany. In this paper, it is shown that these MDCDs strongly depend on the sensor quality (for which an analytical form of the Gaussian error overbound of the sensor error is derived) and on the train dynamics (velocity). This analysis shows for two detectors very promising results and suggests a possible optimal combination of their test statistics.**

I. Introduction

Global Navigation Satellite Systems (GNSS) are inspiring more and more safety of life applications like aviation, maritime and railway. However, for terrestrial applications in general and for rail applications especially, the signals provided by satellites are often blocked and reflected by surrounding obstacles like trees, terrain and buildings. So the signals coming to the receiving GNSS antenna might not be the direct signals but distorted ones. This has a huge impact on the achievable position accuracy, system availability, continuity and integrity. Consequently, pure satellite based navigation/localization systems may fail to provide the required system performance particularly for safety-of-life critical railway applications. Furthermore, GNSS is generally delivering an absolute positioning which is often not what matters in rail navigation. Here, trains can only move on well-defined smooth tracks and the localization objective consists of determining on which track segment and at which level in this segment the train is located and in which direction it moves. This information is crucial for collision avoidance system such as RCAS[1]. In case the position of the trains within the track map is reliably and continuously known, possible train collision situations can be identified and avoided on time.

There are different approaches to solve this localization problem: The two main methods are map matching and dead reckoning system. The former obtains an absolute 3D position estimating using GNSS and additional sensors for each epoch and matches this position with the track map. This could be done by choosing the closest point in the track as the best estimate. In the second approach, the movement of the train relatively to a reference point is estimated incorporating all available sensors. Hence the position within the map is directly known. This approach can provide a more accurate and reliable solution since no intermediate solution is computed. Train localization/navigation using GNSS and IMU has been investigated by many different authors some of them providing novel and promising techniques using Bayesian filters [6].

One of the most critical situations for dead reckoning systems are switches. Here, the train localization system needs to detect reliably and automatically with low latency which track was taken by the train. This decision can be done by determining the curvature of the track. In [1], low-cost MEMS gyroscopes are used for curvature detection. By applying a matched filter, the detection is optimized for real-time operations. However, the reliability of the detection cannot be determined which is mandatory for integrity assessment.

In this paper, we define and investigate the usage of three different test statistics to classify the curvature of the track instantaneously. We also address the performance of this classification with respect the false alert and miss-detection probabilities. Based on these results, we determine the minimum velocity which is necessary to reliably identify the curvature. In our approach, we use three inertial sensor components, i.e., an along-track and a cross-track accelerometer and a heading rate gyroscope. As a matter of course, the classification perfor-

[1]Railway Collision Avoidance System (RCAS) - a project of the German Aerospace Center (DLR) - investigating, developing and validating a 'safety overlay' system which can be deployed on top of any existing safety infrastructure in train networks. The core idea of RCAS is to broadcast the position and intended track of trains as well as additional information like vehicle size to all other trains in the area using an ad-hoc train-to-train communication system. This enables train drivers to have an up-to-date accurate knowledge of the traffic situation in the vicinity, and act in consequence.

mance depends strongly on the quality of the sensor. Hence, we discuss the sensor error model, derive the corresponding stochastic differential equation and the Gaussian overbound of the stochastic process solution. We then outline and analyze the three possible curvature computation methods expressed as ratios of sensor outputs. Later the resulting test statistics of these three methods are evaluated with respect to standard German track curvatures. Finally, we conclude this paper with a summary and a direction for future work.

II. System Model

A. General System Assumption

In this paragraph we list the major assumptions that we make except those related to the error model extensively discussed in the following section.

We neglect the effect of the gravity related errors in the inertial sensors. That is we assume that the plan of motion (formed by the along track and cross track vectors) is perpendicular to the gravity vector. Hence, the acceleration due to the gravity is not measured by the along and cross track sensors. This assumption might be valid due to the planar construction requirement of switches in general.

We assume that the accelerometers are perfectly aligned with the body frame of the train. Hence, no along track and cross track misalignment are considered.

For the heading rate gyroscope, we further assume a perfectly alignment of the motion plan. We further assume a perfect correction of the turn rate errors due to the Coriolis force and the earth rotation.

B. Inertial Sensor Error Model

Inertial error models have been widely discussed in the literature. According to [2], however it is sufficient to use a simplified version of sensor model. Assuming the misalignment of the different sensors with respect to the reference axes are known, the measured sensor output can be written as:

$$\hat{m}(t) = (1+s_f)m(t) + b(t), \tag{1}$$

where $\hat{m}(t)$ is the measured sensor output such as angular turn rate and a 1-D acceleration, respectively. The true value of this quantity is denoted as $m(t)$ and can be used as the input value in the simulations. It is possible to simulate different type of scenarios as for example vibrations or constant acceleration, deceleration [5]. An ideal accelerometer would directly sense $m(t)$ but in a non ideal case, the measured acceleration or turn rate is decomposed into a proportional part (proportional to a scaling factor s_f) and a time dependent drift part $b(t)$. The latter can be modeled by a constant offset b_0 as well as a time varying $b_1(t)$ and a sampling noise component η_m:

$$b(t) = b_0 + b_1(t) + \eta_m. \tag{2}$$

We assume that the offset b_0 stays constant during each run and is corrected by an initial calibration of the sensors. Additionally, the sampling noise is assumed to be Gaussian distributed with zero-mean and a variance σ_m^2. The time-varying component is represented by a 1st-order Gauss-Markov process which can be expressed mathematically by

$$\dot{b}_1(t) = -\frac{1}{\tau} b_1(t) + \eta_b, \tag{3}$$

where τ is the correlation time and η_b is the driving noise which can be assumed to be Gaussian distributed with zero mean and variance σ_b^2. This is also known as an Ornstein-Uhlenbeck process with a rate of mean reversion of $\frac{1}{\tau}$ and a volatility σ_b.

In order to obtain realistic values for the sampling and driving noise component as well as for the time correlation, real sensor measurements have to be analyzed with the help of the Allan variance and auto-correlation function of a long series of zero-input measurements [2]. Exemplary, we show the resulting parameters of three different qualities of inertial sensors in Table 2. We will use these parameters and values throughout our paper.

C. Stochastic Differential Equation and its Solution

Due to the focus of this paper, we need to investigate not only the error of the measurement itself but also its propagation via integration. In the following, we look into the stochastic differential equation issues to solve our problem.

Let us first consider a one dimensional translational acceleration (without attitude change) only. The position of the rover can be determined using only one accelerometer or the combination of redundant accelerometers in the direction of the acceleration. We combine the Equation (1) and (2) and obtain:

$$\hat{m}(t) = (1+s_f)m(t) + b_0 + b_1(t) + \eta_m, \tag{4}$$

Let the error of the measurement be noted by $\Delta\hat{m}(t)$ with:

$$\begin{aligned} \Delta\hat{m}(t) &= \hat{m}(t) - m(t) \\ &= s_f m(t) + b_0 + b_1(t) + \eta_m. \end{aligned} \tag{5}$$

The time-varying bias $b_1(t)$ is the solution of the stochastic differential Equation (3). If we rewrite this equation into the Ito-form and introduce a one-dimensional Brownian motion B_t, we obtain for the sensor time-varying bias the following [9]:

$$db_1(t) = -\frac{1}{\tau} b_1(t)dt + \sigma_b dB_{t,1}. \tag{6}$$

The corresponding error $u(t)$ introduced by the integration of the measurement error can be expressed by:

$$du(t) = \left(s_f m(t) + b_0 + b_1(t)\right)dt + \sigma_m dB_{t,2} \tag{7}$$

These equations can be applied to all our measurements required for our test statistics, i.e., to the cross track and along track accelerometer as well as to the heading rate gyroscope.

In order to solve our problem, let us define a state vector $\boldsymbol{x}(t) = (b_1(t) \quad u(t))^T$. By applying the previous defined equations, we can rewrite our problem as follows:

$$d\boldsymbol{x}(t) = \begin{pmatrix} db_1(t) \\ du(t) \end{pmatrix} = \boldsymbol{\beta}_t(\boldsymbol{x}(t))dt + \boldsymbol{S}\ d\boldsymbol{b}_t, \tag{8}$$

with $\boldsymbol{\beta}_t(\boldsymbol{x}(t)) = \left(\begin{pmatrix}-1/\tau\\1\end{pmatrix} b_1(t) + \begin{pmatrix}0\\ s_f m(t)+b_0\end{pmatrix}\right)$,
$\boldsymbol{S} = \begin{pmatrix}\sigma_b & 0\\ 0 & \sigma_m\end{pmatrix}$ and $d\boldsymbol{b}_t = (dB_{t,1} \quad dB_{t,2})^T$.

In general, two different approaches are used to solve these kind of problems. The first one uses a generator of the Ito-diffusion process defined by the stochastic differential equation and derive a partial differential equation, so called Kolmogorov Forward Equation or Fokker Planck Equation. Its solution is a transition probability density function of the solution process (see [4] and [3]).

The second method takes advantage of the fact that the process solution is Gaussian distributed, if the initial state densities can be assumed to be also Gaussian distributed. Hence, it is sufficient to investigate the evolution of the corresponding expectation and variance of the transition density function. In the section below, we apply the second concept and discuss the results.

D. Analytical Form of the Transition Density solution of the Stochastic Differential Equation

We consider a state vector comprising the drift of the sensor and the integral with respect to time of the sensor error (e.g., the velocity error for an accelerometer or the heading error for an angle rate gyro). So we need to solve this problem:

$$\boldsymbol{x}(t) = \boldsymbol{x}(0) + \int_0^t \boldsymbol{\beta}_l(\boldsymbol{x}(l))\,dl + \boldsymbol{S}\,d\boldsymbol{b}_t,$$

where $\boldsymbol{x}(0) = (b_1(0) \qquad u(0))^T$ is our initial state vector. Recall from before that this can be considered as an Ornstein-Uhlenbeck process in case of a continuous time problem or as an 1st-order auto-regressive process with equilibrium at 0 in case of a discrete time problem. Thus, we can reformulate Equation (6) as integrated process:

$$b_1(t) = b_1(0)e^{-\frac{t}{\tau}} + \sigma_b \int_0^t e^{\frac{l-t}{\tau}} dB_{l,1}.$$

Under the assumption that the initial value of the time-variant bias $b_1(0)$ can be considered as normal distributed random variable with mean $\mathscr{E}[b_1(0)] = \mu_{b_{1,0}}$ and variance $\mathscr{V}[b_1(0)] = \sigma^2_{b_{1,0}}$, the solution of the bias differential equation results also in a Gaussian distributed quantity, where the corresponding mean and variances are given by:

$$\mathscr{E}[b_1(t)] = \mu_{b_{1,t}} = \mu_{b_{1,0}} e^{-\frac{t}{\tau}}$$
$$\mathscr{V}[b_1(t)] = \sigma^2_{b_{1,t}} = \frac{\tau}{2}\sigma_b^2\left(1 - \exp\left(-\frac{2t}{\tau}\right)\right) + \sigma^2_{b_{1,0}}\, e^{-\frac{2t}{\tau}}$$

Similar steps, we can apply to the full stochastic differential equation $\boldsymbol{x}(t) = (b_1(t) \quad u(t))^T$ and we obtain:

$$\boldsymbol{x}(t) = \begin{pmatrix}e^{-t/\tau} & 0\\ 0 & 1\end{pmatrix}\boldsymbol{x}(0) + \boldsymbol{h}(t) + \begin{pmatrix}0\\ \sigma_m B_{t,2}\end{pmatrix},$$

where $\boldsymbol{h}(t) = \begin{pmatrix}\sigma_b \int_0^t e^{\frac{l-t}{\tau}} dB_{l,1}\\ \int_0^t (s_f m(l) + b_0 + b_1(l))\,dl\end{pmatrix}$. To solve our problem, we propose to compute the expectation and variance of the process in a snapshot manner, i.e., for each time step. So, for the expectation we have to solve:

$$\begin{aligned}\mathscr{E}[\boldsymbol{x}(t)] &= \mathscr{E}[\boldsymbol{x}(0)] + \mathscr{E}\left[\int_0^t \boldsymbol{\beta}_l(\boldsymbol{x}(l))\,dl\right] + \mathscr{E}[\boldsymbol{S}\ \boldsymbol{b}_t]\\ &= \mathscr{E}[\boldsymbol{x}(0)] + \int_0^t \mathscr{E}[\boldsymbol{\beta}_l(\boldsymbol{x}(l))\,dl],\end{aligned}$$

since $\mathscr{E}[\boldsymbol{b}_t] = (0 \quad 0)^T$ by definition of a Brownian motion. The two components of the sum can be rewritten as:

$$\mathscr{E}[\boldsymbol{x}(0)] = \begin{pmatrix}e^{-t/\tau} & 0\\ -\tau(e^{-t/(\tau-1)}) & 1\end{pmatrix}\begin{pmatrix}\mu_{b_{1,0}}\\ \mu_{u_0}\end{pmatrix}$$
$$\int_0^t \mathscr{E}[\boldsymbol{\beta}_l(\boldsymbol{x}(l))\,dl] = \begin{pmatrix}0\\ s_f\int_0^t m(l)\,dl + b_0 t\end{pmatrix}$$

The derivation of the corresponding state vector covariance matrix is quite complex, so we just want to state the result here in this paper.

$$\mathscr{V}[\boldsymbol{x}(t)] = \begin{pmatrix}c_{11}(t) & c_{12}(t)\\ c_{21}(t) & c_{22}(t)\end{pmatrix}. \tag{9}$$

Please note that the covariance matrix is symmetric, i.e., $c_{12}(t) = c_{21}(t)$. Also we define an auxiliary Gaussian random variable $\varepsilon_\tau(t) = \int_0^t \int_0^r e^{\frac{l-r}{\tau}} dB_{l,1} dr$. So, we get

$$\begin{pmatrix}c_{11}(t)\\ c_{22}(t)\\ c_{22}(t)\end{pmatrix} = \begin{pmatrix}e^{-2t/\tau} & 0\\ \tau^2(e^{-t/\tau}-1)^2 & 1\\ -\tau(e^{-2t/\tau} - e^{-t/\tau}) & 0\end{pmatrix}\begin{pmatrix}\sigma^2_{b1,0}\\ \sigma_{u,0}\end{pmatrix} + \\ + \begin{pmatrix}\tau/2(1-e^{-2t/\tau}) & 0\\ \sigma^2_{\varepsilon_\tau(t)} & t\\ \mathscr{E}\left[\varepsilon_\tau(t)\int_0^t e^{\frac{l-t}{\tau}} dB_{l,1}\right] & 0\end{pmatrix}\begin{pmatrix}\sigma_b^2\\ \sigma_m^2\end{pmatrix}.$$

Recall that $\varepsilon_\tau(t)$ is function of $B_{t,1}$, we kept the cross products as non necessarily zero terms. In fact (See Appendix A for more details), the mean $\mathscr{E}\left[\varepsilon_\tau(t)\int_0^t e^{\frac{l-t}{\tau}} dB_{l,1}\right] = \frac{1}{2}\tau^2 - \frac{\tau^2}{e^{\frac{t}{\tau}}} + \frac{\tau^2}{2e^{2\frac{t}{\tau}}}$, and the variance of $\varepsilon_\tau(t)$ is given by $\sigma^2_{\varepsilon_\tau(t)} = t\tau^2 - \frac{3}{2}\tau^3 + 2\frac{\tau^3}{e^{\frac{t}{\tau}}} - \frac{\tau^3}{2e^{2\frac{t}{\tau}}}$

Finally we observe that the covariance matrix $\mathscr{V}[\boldsymbol{x}(t)]$ is not diagonal in the general case.

We observe that when the random variables in the model of the sensor are all Gaussian distributed (including the initial point $b_1(0)$ and $u0$, the state vector is also Gaussian distributed. Therefore the propagation of the mean and the variance is sufficient if we want to characterize the whole distribution.

Given all these expressions, we can deduce the expectation and the variance of the state vector as function of time t, time constant τ and the parameters of the problem.

$$\mathscr{E}[b_1(t)] = \frac{\mu_{b10}}{e^{\frac{t}{\tau}}}$$
$$\mathscr{E}[u(t)] = I_{st}s_f + b_0 t + \mu_{b10}\tau - \frac{\mu_{b10}\tau}{e^{\frac{t}{\tau}}} + \mu_{u0}$$
$$\mathscr{V}[b_1(t)] = \frac{1}{2}\sigma_b^2\tau - \frac{\sigma_b^2\tau}{2e^{2\frac{t}{\tau}}} + \frac{\sigma_{b10}^2}{e^{2\frac{t}{\tau}}}$$
$$\mathscr{V}[u(t)] = \sigma_b^2 t\tau^2 - \frac{3}{2}\sigma_b^2\tau^3 + 2\frac{\sigma_b^2\tau^3}{e^{\frac{t}{\tau}}} - \frac{\sigma_b^2\tau^3}{2e^{2\frac{t}{\tau}}} + \sigma_{b10}^2\tau^2 - 2\frac{\sigma_{b10}^2\tau^2}{e^{\frac{t}{\tau}}} + \frac{\sigma_{b10}^2\tau^2}{e^{2\frac{t}{\tau}}} + \sigma_m^2 t + \sigma_{u,0}^2$$

By using Equation (5), we deduce the expectation and the variance of the sensor error:

$$\mathscr{E}[\Delta\hat{m}_t] = s_f m(t) + b_0 + e^{-\frac{t}{\tau}}\mu_{b10}$$
$$\mathscr{V}[\Delta\hat{m}_t] = \frac{1}{2}\sigma_b^2\tau - \frac{\sigma_b^2\tau}{2e^{2\frac{t}{\tau}}} + \frac{\sigma_{b10}^2}{e^{2\frac{t}{\tau}}} + \sigma_m^2$$

III. Snapshot Track Curvature Classification

A. Curvature Determination

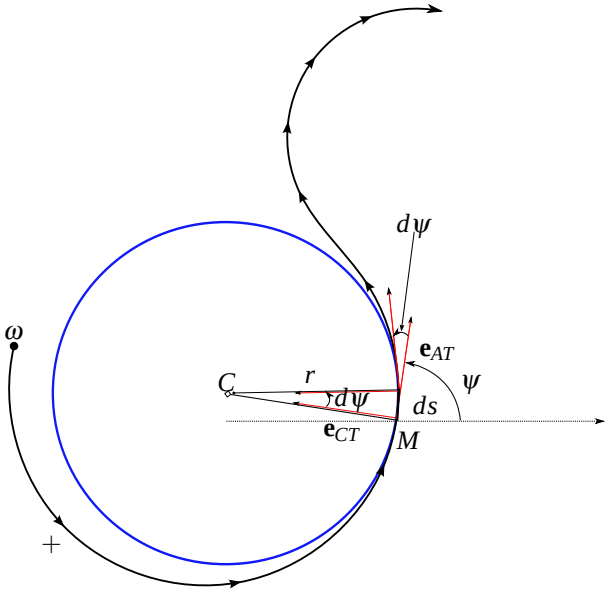

Figure 1: Display of the 2D curvilinear coordinate system to determine the track curvature.

In the following section, the physical assessment of the track curvature is introduced and three different methods are outlined. Let $s(t)$ being the curvilinear abscissa representing the length of the arc represented by the track from a reference position to a current point. The velocity vector of the train is $\mathbf{v} = \dot{s}\mathbf{e}_{AT}$ and the acceleration vector is:

$$\mathbf{a} = \frac{d\mathbf{v}}{dt} = \frac{d(\dot{s}\mathbf{e}_{AT})}{dt} = \ddot{s}\mathbf{e}_{AT} + \dot{s}\dot{\mathbf{e}}_{AT} \tag{10}$$

In this expression and in the rest of this chapter we drop the time t for simplification. The dot above variables always means the derivative of the given variable with respect to time. To express $\dot{\mathbf{e}}_{AT}$, we use the notations of Figure 1. During dt, the point M moved from s to $s+ds$ and the unit along track vector has rotated with the angle $d\psi$. This drives to the following relation:

$$\dot{\mathbf{e}}_{AT} = \dot{\psi}\mathbf{e}_{CT}$$

Observing that the acceleration vector lies in the osculating plan defined by $(\mathbf{e}_{AT}, \mathbf{e}_{CT})$, we can decompose the acceleration into 2 components: and taking the same notation as for the unit vectors, we have:

$$\mathbf{a}(t) = a_{AT}\mathbf{e}_{AT} + a_{CT}\mathbf{e}_{CT}$$

$$a_{AT} = \ddot{s}$$
$$a_{CT} = \dot{s}\dot{\psi}$$

We observe that $\dot{s} = r\dot{\psi}$, so we have the following expression:

$$a_{CT} = r\dot{\psi}^2 \tag{11}$$

With r being the local radius of the trajectory.

We observe that Equation (11) can be expressed in terms of $\dot{s}$ rather than $\dot{\psi}$ and observing that $\|\mathbf{v}\| = \dot{s}$, we have:

$$a_{CT} = \frac{\|\mathbf{v}\|^2}{r} \tag{12}$$

There is a relation between the speed of the train, the cross track acceleration and the heading rate for a given trajectory.

We have the following relations:

$$a_{CT} = r\dot{\psi}^2 = \frac{\|\mathbf{v}\|^2}{r} \tag{13}$$

In this equation, we can directly sense the cross track acceleration a_{CT}, the heading rate $\dot{\psi}$ and indirectly the velocity of the train $\mathbf{v}$ (integral of the along track acceleration). This is an important a-priori information that can be used in a test statistic to decide which direction the train has taken after a switch. By convention we will choose to work with the curvature rather than with r. Let $\kappa = 1/r$ the relation above can be written as follows:

$$a_{CT} = \frac{\dot{\psi}^2}{\kappa} = \kappa\|\mathbf{v}\|^2 \tag{14}$$

In this equation, κ can be obtained in three different ways:

$$\kappa_1 = \frac{\dot{\psi}^2}{a_{CT}} \tag{15}$$

$$\kappa_2 = \frac{|\dot{\psi}|}{\|\mathbf{v}\|} \tag{16}$$

$$\kappa_3 = \frac{a_{CT}}{\|\mathbf{v}\|^2} \tag{17}$$

All three methods can also be used in a non-stationary scenario, i.e., while the train is moving. Otherwise the curvature

determination might be not defined. That is if $a_{CT} = 0$, κ_1 is undefined and if $\|\mathbf{v}(t)\| = 0$, κ_2 and κ_3 are undefined.

B. Test Statistic

In this section, we analyze the resulting test statistic based on the three curvature determination methods. To compute $\kappa_i, i = 1,\ldots,3$, we need the heading rate, along-track and cross-track accelerations. These measurements are distorted by sensor errors which can be modeled as described in Section II-B. Using the SDE results from Section II-C, we can access the error distribution of each measurement required to determine the curvature. However, the distribution of curvatures itself is not simple to derive since we have to obtain the distribution of a ration of random variables. The resulting distribution might not be symmetric and can be even heavy tailed. In the following, we discuss the expected behavior of the test statistics.

Naturally, if all measurements would be error-free, all three curvature computations would deliver the same result $\kappa_1 = \kappa_2 = \kappa_3$. But due to the randomness of the measurements of $a_{CT}(t)$, $\dot{\psi}(t)$ and $\mathbf{v}(t)$, the performance of the obtained curvatures can only be characterized in terms of distribution.

First method κ_1: The measurements of this methods can be directly sensed, so no integration of the measurements is required. However, we can see that if the curvature of the path is zero, i.e., the track is straight, the numerator will take positive random values following a χ^2 distribution and the denominator will take values centered at 0. This induces fat tails in the distribution of κ_1. Consequently, it might be not very promising to use this method for the hypothesis test.

Second method κ_2: Here, we observe a ratio between a normally distributed random variable and a folded normal distribution (the absolute value of a normally distributed random variable). In the case of a ratio between two independent, normally distributed random variables with zero mean, the distribution of the ratio follows a Cauchy distribution. In the case of non-centered distributions, it has been demonstrated [7] that the probability density function can be written as follows:

$$p_{K_2^*}(\kappa_2^*) = \frac{\alpha \exp\left\{\frac{1}{2}\frac{\alpha^2}{\gamma} - \frac{1}{2}\xi\right\}}{\gamma^3}\frac{1}{\psi} \times \left(2\Phi\frac{\alpha}{\gamma} - 1\right) + \\ + \frac{1}{\gamma\pi\psi}\exp\left\{-\frac{1}{2}\xi\right\}, \tag{18}$$

where

$$\alpha = \frac{\mathscr{E}[\dot{\psi}]}{\mathscr{V}[\dot{\psi}]}\kappa_2 + \frac{\mathscr{E}[v]}{\mathscr{V}[v]}$$
$$\gamma = \frac{1}{\mathscr{V}[\dot{\psi}]}\kappa_2^2 + \frac{1}{\mathscr{V}[v]}$$
$$\xi = \frac{\mathscr{E}[\dot{\psi}]^2}{\mathscr{V}[\dot{\psi}]} + \frac{\mathscr{E}[v]^2}{\mathscr{V}[v]}$$
$$\psi = \sqrt{\mathscr{V}[\dot{\psi}]\mathscr{V}[v]}$$

and $\kappa_2^* = \frac{\dot{\psi}(t)}{\mathbf{v}(t)}$, and $\Phi(u) = \int_{-\infty}^{u}\frac{1}{\sqrt{2\pi}}\exp\left\{-\frac{1}{2}z^2\right\}dz$. This expression is not representing the test statistic of interest κ_2 for which no closed form could be found.

Third method κ_3: Similar to κ_2, to nominator can be seen as normal distributed random variable. However, the denominator is not only linear dependent on an folded normal distributed random variable, but quadratically dependent. Also in this case no close for solution can be found.

In the remaining paper, we assess the distributions of $\kappa_i, i = 1,\ldots,3$ via Monte-Carlo simulations. As derived before we can compute the probability distributions of $a_{CT}(t)$, $\dot{\psi}(t)$ and $\mathbf{v}(t)$ depending on the quality of the sensor as well as initialization. Please note that the direct use of heavy tailed distributions can generate instabilities of the test statistics. In this case, the mean and variance may not exist especially in the case of high densities around zero for the test statistics denominators.

One possibility is to exclude the samples of $a_{CT}(t)$, $\|\mathbf{v}(t)\|$ and $\|\mathbf{v}(t)\|^2$ that are close to zero, or in an interval around zero. The area to exclude using a pretest should not be too large for one reason essentially: the exclusion reduces the availability of the test statistics (for each sample falling in the excluded area, the corresponding test statistics is set as unavailable). But the closer the exclusion bounds are to zero, the wider the distribution of the test statistics and therefore the smaller the minimum detectable curvature difference (MDCD).

C. Hypothesis Test

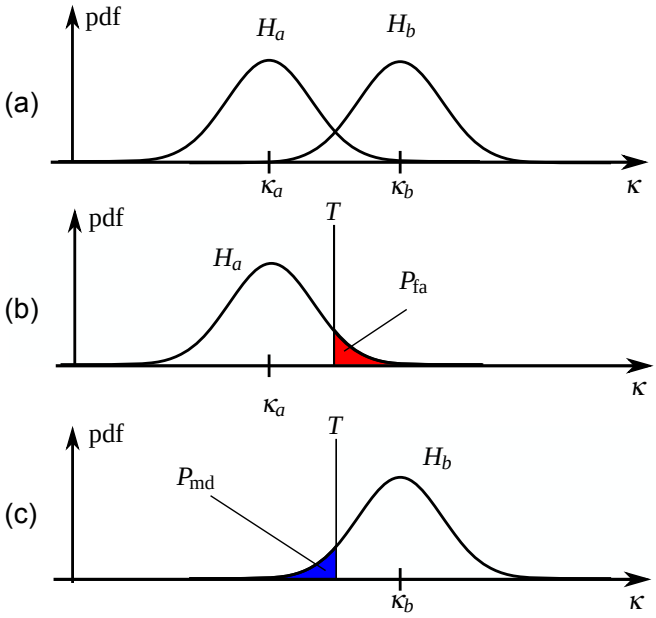

Figure 2: Curvature error distribution for different hypotheses.

To classify or identify a certain curvature, we compare our computed curvature with a threshold. The latter, we have determined by a standard hypothesis test algorithm. In the following, this algorithm is described briefly.

First of all, reliable knowledge of curvature determination error behavior is required. We denoted this curvature error probability density function as $p_K(\kappa)$. We assume that this

pdf is centered at the true curvature. Then we can define the distributions for two different track curvature hypotheses that we want to test. For example, after a switch a train might have two possibilities to move on, i.e., track segment one with curvature κ_a or track segment two with curvature κ_b. Figure2 (a) illustrates the resulting curvature pdfs, if either track segment one $p_K(\kappa|H_a)$ or track segment two $p_K(\kappa|H_b)$ has been taken. In order to make a decision, we have to define a threshold T against which we compare our curvature measurements. If our measurement is below the obtained threshold, we decide for H_a and if it exceeds this threshold, we decide for H_b. To find this threshold we have to consider the probability of false alarm P_{fa}. This probability is a system reliability requirement and accounts for the case, where we decided for H_b (indicated segment two, while hypothesis H_a was correct (the train took the segment one). This is depicted on Figure 2 (b)). Consequently, the threshold is given by

$$T = \arg\left(P_{\text{fa}} = P_K(\kappa > T|H_a) = \int_T^\infty p_K(\kappa|H_a)d\kappa\right).$$

Similar considerations can now be done for hypothesis H_b as well. A probability of missed detection, i.e., we decided for segment one while the train took segment two, is normally defined as

$$P_{\text{md}} = P_K(\kappa < T|H_b) = \int_{-\infty}^T p_K(\kappa|H_b)d\kappa.$$

This is displayed in Figure 2 (c). P_{md} is also a system reliability requirement and normally pre-defined by the system. So for a given P_{md}, we can find a κ_m such that

$$\kappa_m = \arg\left(\int_T^\infty p_K(\kappa|H_m)d\kappa = P_{\text{md}}\right),$$

where H_m is the hypothesis that the train has taken a track with curvature κ_m. Thus, we can define a minimum detectable curvature difference $\text{MDCD} = \kappa_m - \kappa_a$ for the given system requirements of false alert and missed detection. Both probabilities, P_{md} and P_{fa} indicate that a wrong decision is made. Since we want to protected hypothesis H_a and H_b equally, we set $P_{\text{fa}} = P_{\text{md}} = P_{\text{WD}}$, where WD stands for wrong decision.

In Figure (3), we show two histograms observed while using the test statistics of κ_3. The train moves with a speed of 50 [km/h] and the coasting time is 75 seconds. By coasting time we understand the time for which the inertial sensors run free, so the time after initialization. We assume that during the coasting period, the speed is obtained by integrating the along track acceleration. In blue, we show the distribution of the test statistic under the hypothesis H_a (with a curvature radius of 10 km) and the red curve corresponds to the hypothesis H_b (with a curvature radius of 1749 m). So the minimum detectable curvature difference is equivalent to $\text{MDCD} = 1/1749 - 10^{-4} = 4.7176 \times 10^{-04}$ [m^{-1}]. The probability of wrong detection is set to $P_{\text{wd}} = 10^{-5}$ and is generally a requirement based on the level of hazard for being on another track than the one expected. This risk is usually defined as a probability of being in this hazardous situation during a predefined exposure time.

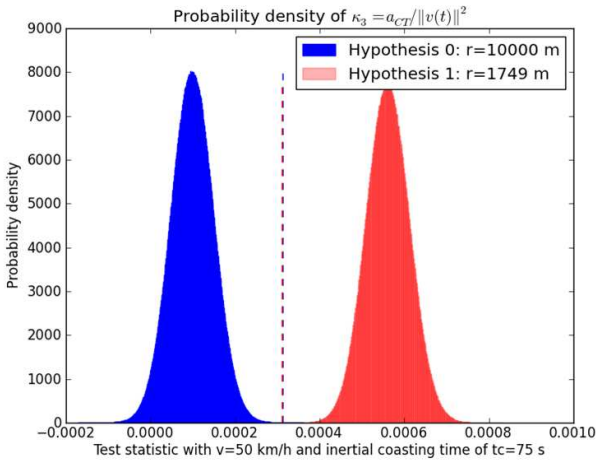

Figure 3: Test statistic κ_3 for two different hypothesis: In blue $\kappa = 10^{-4}$ [m^{-1}] and in red $\kappa = 1/1749$ [m^{-1}] which correspond to a minimum detectable curvature difference of $\text{MDCD} = 4.7176 \times 10^{-04}$ [m^{-1}] with $P_{wd} = 10^{-5}$.

IV. Simulation and Evaluation

A. Simulation Environment

For simulation, we used standard curvatures found in the German railway. A summary of available curvatures and corresponding maximum allowed train velocity can be found in Table 1. As mentioned before, the error model parameters of the used inertial sensors are shown in Table 2.

Table 1: Basic Design Parameters of German standard switches [8]

radius r in m	curvature c in 10^{-3} 1/m	max velocity v_{max} in km/h
190	5.26	40
300	3.33	50
500	2.0	60
760	1.32	80
1200	0.83	100
2500	0.4	120

We propose to investigate a curvature detector based on the three test statistics defined in Equations (15, 16, 17). The path identification after a switch is crucial for train surveillance and train collision avoidance systems. If we assume not to know the itinerary but just the map with the switch locations and the curvature of the possible paths after the switches, it is possible to determine the path followed by the train with a confidence depending on the quality of the sensors.

In the simulations, we use a sensor having the following characteristics:

We solve the stochastic differential system for the expectation and the variance for all three different sensor grades.

We draw paths following the process distributions calculated and we build the histograms for each test statistic κ_1, κ_2 and κ_3.

The initial along track velocity uncertainty might be given by GNSS and is assumed to have a $\sigma_{\hat{v}(0)}0 = 0.05$ [m/s].

Table 2: Sensor error model parameter developed in [2] for three different classes of IMU grades, i.e., tactical, automotive and consumer grade IMUs. The notation can be read as following the sampling noise is denoted by σ_w, whereas the noise of the time variant bias is represented by σ_{b_1} and its time constant by τ.

Sensor		σ_m	σ_{b_1}	τ
Gyro	Tactical	0.0017 deg/s	0.35 deg/hr	100 s
	Auto.	0.05 deg/s	180 deg/hr	300 s
	Consumer	0.05 deg/s	360 deg/hr	300 s
Acc	Tactical	50×10^{-5} g	50×10^{-6} g	60 s
	Auto.	1×10^{-3} g	1.2×10^{-3} g	100 s
	Consumer	1×10^{-3} g	2.4×10^{-3} g	100 s

When GNSS is not longer available, the velocity is drifting from its initial value considering a coasting using along track accelerometer.

B. Assumptions for train localization

At a given initial epoch we assume to know the position and the direction of displacement of the train (for example at the departure station). The localization problem consists of determining the track segment ID, the direction of displacement and the curvilinear abscissa on the track segment.

A track segment is defined as a path between two switches. We assume that between two guaranteed positions (e.g., obtained by GNSS and verified by a receiver autonomous integrity monitoring), velocity fixes a coasting with the inertial unit based on along track, cross track accelerometers and a heading rate gyro using the characteristics defined in Table 2. The coasting time is not longer than 1 second when at least 5 satellites are visible which is generally the case. But in some cases (long tunnels or in the general case of bad satellite visibility or when the satellite signals are blocked or reflected by a strong multipath environment) the coasting time could be last much longer (up to several minutes). Nevertheless, as long as the information used is not integrated in the time to obtain velocity, position or heading angle, the error in the information is stationary and can be overbounded by a Gaussian distribution for a non zero required integrity risk. This overbound remains constant assuming the error is a stationary process.

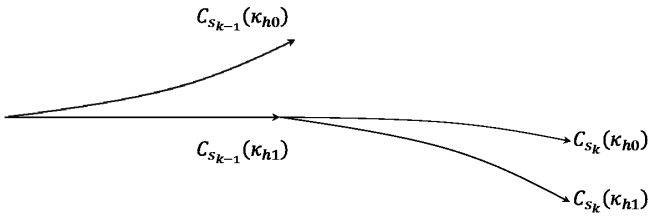

Figure 4: Tracks configuration assumption

In Figure (4) we show the topology we adopt for the switch scenario. We assume at each switch, only two possible tracks can be taken.

C. Minimum Detectable Curvature Difference

We have seen in the precedent section that the probability of wrong decision is an important system reliability requirement. The question we need to answer is now: What is the minimum curvature difference for which we can detect an alternative curvature with a probability of $1-P_{\mathrm{WD}}$? In order to answer this question, we first have to determine our test statistic threshold $T=\mathrm{fct}(\kappa_0,P_{\mathrm{WD}})$ which is a function of the curvature of our H_a hypothesis κ_0 and the allowed probability of false alert. Then we generate the probability density function for a continuously growing curvature $\kappa_m>\kappa_0$ until we get:

$$\int_{-\infty}^{T} p_K\left(\kappa_i|H_m\right)d\kappa_i = P\left(\kappa_i<T|H_m\right), \tag{19}$$

where H_m is the hypothesis centered at κ_m and κ_i, for $i=1,\ldots,3$ are the different test statistics defined in Equation (15, 16,17). Finally, the MDCD is $\kappa_m-\kappa_0$.

The MDCD is a function of the velocity of the train. Intuitively the larger the velocity of the train, the smaller the dispersion of the test statistic.

We investigate the MDCD for each test statistic as function of the train velocity at a switch and for different IMU qualities. In the following investigations, we set our curvature of hypothesis H_a to $\kappa_0=10^-4$ [m^{-1}].

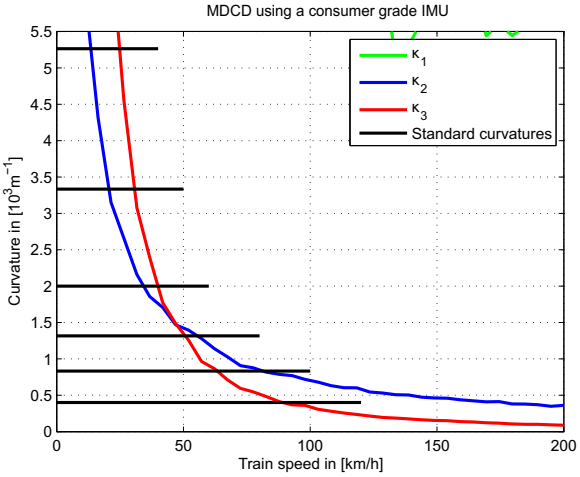

Figure 5: Minimum detectable curvature difference with respect to $\kappa_0=10^-4$ [m^{-1}] obtained for the three different curvature determination methods κ_1, κ_2 and κ_3 vs. velocity are shown. For comparison, the standard German curvatures and their max. velocities are indicated by black lines. This plot is valid for a $P_{\mathrm{wd}}=10^{-5}$ and using consumer grade sensors.

In Figures (5, 6, 7) we have plotted the corresponding MDCD vs. the velocity for each test statistic and for each IMU quality. The black horizontal lines represent the standard curvatures of tracks observed in Germany. Each standard line starts at $v=0$ [km/h] and stop at the maximal allowed velocity for the corresponding curvature. The larger the curvature, the smaller the maximal allowable speed. The initial and reference curvature to be almost zero (a curvature of exactly 0 lends to

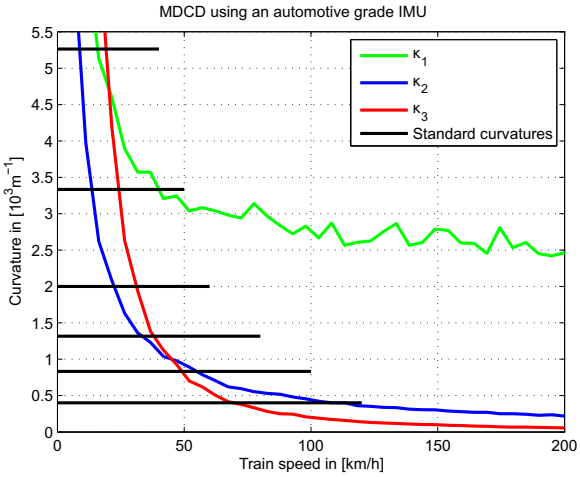

Figure 6: Minimum detectable curvature difference with respect to $\kappa_0 = 10^-4$ [m^{-1}] obtained with the three different curvature determination methods κ_1, κ_2 and κ_3 vs. velocity are shown. For comparison, the standard German curvatures and their max. velocities are indicated by black lines. This plot is valid for a $P_{wd} = 10^{-5}$ and using automotive grade sensors.

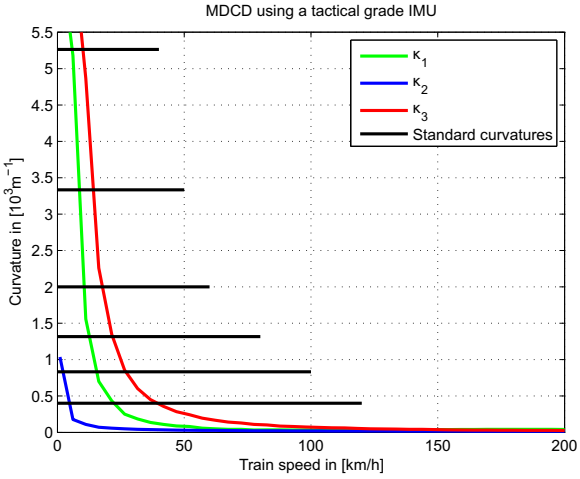

Figure 7: Minimum detectable curvature difference with respect to $\kappa_0 = 10^-4$ [m^{-1}] obtained with the three different curvature determination methods κ_1, κ_2 and κ_3 vs. velocity are shown. For comparison, the standard German curvatures and their max. velocities are indicated by black lines. This plot is valid for a $P_{wd} = 10^{-5}$ and using tactical grade sensors.

a singularity). We see that the lower the velocity, the higher the MDCD.

Although κ_1 seems to provide acceptable performance in the case of tactical grade IMU, its low availability for a large range of velocities see Figure (8) makes it unusable for the simulated scenario. Only κ_2 and κ_3 are providing acceptable results (their availabilities were always 100% for any type of IMU).

For tactical grade IMU, we see a very effective κ_2 based test statistic. In fact the combination of high accurate velocity and high performance heading gyro provides a sharp distribution

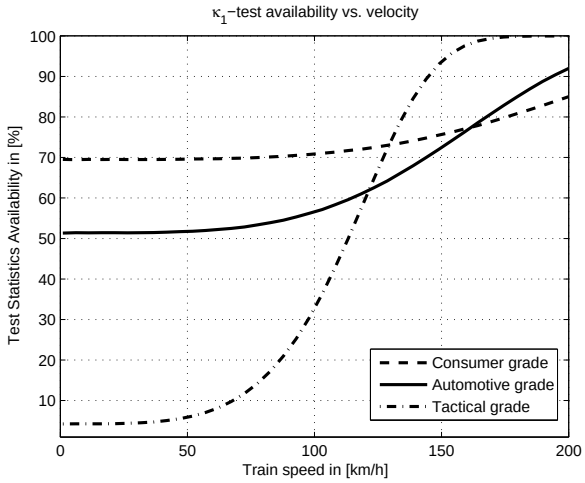

Figure 8: Availability degradation plot of κ_1 vs. velocity. for different IMU grades.

and therefore a clear signature when the train change its track. For this tactical grade IMU, κ_2 and κ_3 are not crossing in the velocity range $[0-200]$ [km/h].

For both the consumer and the automotive grade IMUs, the MDCD curves cross at a speed of approximately 50 [km/h]. This suggests a velocity based test selection: below 50 [km/h] we use κ_2 to make our decision and above this limit, we use κ_3 which performs better. A more efficient strategy could consist of defining a weighted combination of both test statistics enabling even lower MDCD. However, this is beyond the scope of this paper.

The results obtained suggest a weighted sum of κ_2 and κ_3 in order to improve the detectability. Some intrinsic problems may appear because of the dependency of all 3 test statistics. Correlations need to be considered while seeking an optimal combination of curvature types.

V. Conclusion

In this paper we explored three different ways to determine track curvatures. The tests are based on ratios of random variables that can be directly sensed like the heading rate gyro and the cross track acceleration and indirectly sensed like the speed of the train which can be obtained by an integration of the along track acceleration.

The expectation and the variance of the Gaussian overbound of the sensor errors are analytically expressed and the test statistics after pretreatment of the random denominators (exclusion of an interval around zero to prevent heavy tailed distributions) are investigated using Monte Carlo simulations. The minimum detectable curvatures difference is determined for three different classes of IMUs, namely consumer, automotive and tactical grade. The resulting MDCD curves have been compared to standard curvatures and their performance have been assessed.

It is shown that κ_1 in addition to being unavailable a large part of the time (exclusion of the high density around zero of

the cross track acceleration) provides when a bad performance. In comparison, κ_2 and κ_3 show best results with a maximum availability when the train is moving. A performance crossover can be observed for the consumer and automotive grade IMUs. That is κ_3 can outperform κ_2 when the velocity of the train is larger than 50 km/h. However, κ_3 depends on the cross track acceleration which is difficult to sense in a more realistic dynamic scenarios (for a non-perfect horizontal plan of motion, for which the gravity vector may introduce a component in cross track direction). In contrast, κ_2 shows a real improvement as it can be reliably used for a large range of velocities. Furthermore, it has a dependency on the heading rate rather than on the accelerations which makes it more robust to realistic scenarios (non-perfect horizontal displacements).

Future studies will consider a generalization of this concept for a three dimensional tracks (with gravity vector not always perpendicular to the motion plan), misalignment of sensors, transition curvatures. The performance crossover observed for κ_2 and κ_3 for low cost IMUs suggests to use a combination of both test statistics which is investigated in a future paper. Another investigation might consider the minimum probability of wrong detection for a given type of IMU and as function of the speed at the switch. This approach can give the level of safety achieved by different types of IMU.

APPENDIX A
EXPECTATION AND VARIANCE OF BROWNIAN MOTIONS (APPEARING IN THE ANALYTICAL FORM OF THE EXPECTATION AND THE VARIANCE OF THE ALONG TRACK VELOCITY ERROR)

A. Expectation of the Brownian Motion

Consider the following Brownian Motion: $\boldsymbol{x}(t) = B_t \int_0^t B_s ds$, so we can express its expected value as

$$\mathscr{E}[\boldsymbol{x}(t)] = \mathscr{E}\left[B_t \int_0^t B_s ds\right] \tag{20}$$

We define $\Delta t = t/n$ and $t_k = k\Delta t$. The Riemann sum approximation of $\boldsymbol{x}(t)$is:

$$X_{t_n} = B_{t_n} \sum_{k=0}^{n-1} B_{t_k} \Delta t \tag{21}$$

$$\mathscr{E}[X_{t_n}] = \mathscr{E}\left[B_{t_n} \sum_{k=0}^{n-1} B_{t_k} \Delta t\right] \tag{22}$$

$$\mathscr{E}[X_{t_n}] = \Delta t \sum_{k=0}^{n-1} \mathscr{E}\left[B_{t_n} B_{t_k}\right] \tag{23}$$

$$\mathscr{E}[X_{t_n}] = \Delta t \sum_{k=0}^{n-1} (t_n \wedge t_k) \tag{24}$$

where $t_n \wedge t_k = \min(t_n, t_k)$

$$\mathscr{E}[X_{t_n}] = \Delta t \sum_{k=0}^{n-1} t_k \tag{25}$$

$$\mathscr{E}[X_{t_n}] = \Delta t^2 \sum_{k=0}^{n-1} k \tag{26}$$

$$\mathscr{E}[X_{t_n}] = \Delta t^2 \frac{n(n-1)}{2} \tag{27}$$

$$\mathscr{E}[X_{t_n}] = \frac{t^2}{n^2} \frac{n(n-1)}{2} \tag{28}$$

By continuity we have $\mathscr{E}[X_{t_n}] \to \mathscr{E}[\boldsymbol{x}(t)]$ when $n \to \infty$ and

$$\mathscr{E}[\boldsymbol{x}(t)] = \frac{t^2}{2} \tag{29}$$

B. Expectation of $\boldsymbol{x}(t) = \eta_t(\tau) \int_0^t e^{\frac{l-t}{\tau}} dB_{b_1 u}$

With $\eta_t(\tau) = \int_0^t B_r dr - \frac{1}{\tau}\int_0^t \int_0^r e^{\frac{l-r}{\tau}} B_u dl dr$ and $\int_0^t e^{\frac{l-t}{\tau}} dB_{b_1 u} = B_{b_1 t} - \frac{1}{\tau}\int_0^t e^{\frac{l-t}{\tau}} B_{b_1 u} dl$.

$$\begin{aligned}\boldsymbol{x}(t) = &\int_0^t B_t B_r dr - \frac{1}{\tau}\int_0^t \int_0^r e^{\frac{l-r}{\tau}} B_t B_u dl dr - \\ &- \frac{1}{\tau}\int_0^t e^{\frac{r-t}{\tau}} B_r dr \int_0^t B_r dr + \\ &+ \frac{1}{\tau^2}\int_0^t e^{\frac{r-t}{\tau}} B_r dr \int_0^t \int_0^r e^{\frac{l-r}{\tau}} B_u dl dr\end{aligned}$$

$$\begin{aligned}\mathscr{E}[\boldsymbol{x}(t)] = &\int_0^t r dr - \frac{1}{\tau}\int_0^t \int_0^r u e^{\frac{l-r}{\tau}} dl dr - \\ &- \frac{1}{\tau}\int_0^t \int_0^r e^{\frac{r'-t}{\tau}} (r' \wedge r)\, dr dr' + \\ &+ \frac{1}{\tau^2}\int_0^t \int_0^t \int_0^r e^{\frac{r'-t+l-r}{\tau}} (r' \wedge u)\, dl dr dr'\end{aligned}$$

Finally we have:

$$\mathscr{E}[\boldsymbol{x}(t)] = \frac{1}{2}\tau^2 - \frac{\tau^2}{e^{\frac{t}{\tau}}} + \frac{\tau^2}{2e^{2\frac{t}{\tau}}}$$

C. Variance of $\eta_t(\tau)$

We recall that $\eta_t(\tau) = \int_0^t B_r dr - \frac{1}{\tau}\int_0^t \int_0^r e^{\frac{l-r}{\tau}} B_u dl dr$

The expectation of $\gamma_t(\tau)$ is equal to zero. Therefore the variance is:

$$\mathscr{V}[\eta_t(\tau)] = \mathscr{E}\left[\eta_t(\tau)^2\right]$$

$$\begin{aligned}\mathscr{V}[\eta_t(\tau)] = &\frac{t^3}{3} + \mathscr{E}\left[-\frac{2}{\tau}\int_0^t B_r dr \int_0^t \int_0^r e^{\frac{l-r}{\tau}} B_u dl dr\right] + \\ &+ \mathscr{E}\left[\frac{1}{\tau^2}\int_0^t \int_0^r e^{\frac{l-r}{\tau}} B_u dl dr \int_0^t \int_0^r e^{\frac{l-r}{\tau}} B_u dl dr\right]\end{aligned}$$

$$\begin{aligned}\mathscr{V}[\eta_t(\tau)] = &\frac{t^3}{3} - \frac{2}{\tau}\int_0^t \int_0^t \int_0^r e^{\frac{l-r}{\tau}} (r' \wedge u)\, dl dr dr' \\ &+ \frac{1}{\tau^2}\int_0^t \int_0^{r'} \int_0^t \int_0^r e^{\frac{u'-r'+l-r}{\tau}} (u' \wedge u)\, dl dr dl' dr'\end{aligned}$$

$$\mathscr{V}\left[\eta_t(\tau)\right] = t\tau^2 - \frac{3}{2}\tau^3 + 2\frac{\tau^3}{e^{\frac{t}{\tau}}} - \frac{\tau^3}{2e^{2\frac{t}{\tau}}}$$

ACKNOWLEGMENT

The authors would like to thank the DLR's Traffic Management Directorate and the Institute of Communications and Navigation for their support.

REFERENCES

[1] Antoni Broquetas, Adolf Comerón, Antoni Gelonch, Josep M. Fuertes, J. Antonio Castro, Damià Felip, Miguel A. López, and José A. Pulido. Track Detection in Railway Sidings Based on MEMS Gyroscope Sensors. *Sensors*, 12(12):16228–16249, 2012.

[2] Demoz Gebre-Egziabher. *Design and Performance Analysis of a Low-Cost Aided Dead Reckoning Navigator*. PhD thesis, Stanford University, 2004.

[3] Anja Grosch and Boubeker Belabbas. Parameter Study of Loosely Coupled INS/GNSS Integrity Performance. In *Proceedings of IEEE/ION PLANS*, Myrtle Beach, SC, USA, 24-26 Apr 2012 2012.

[4] Anja Grosch, Boubeker Belabbas, and Michael Meurer. Redundant Inertial-Aided GBAS for Civil Aviation. In European Space Research and Technology Centre (ESTEC), editors, *Navitec 2010*, Noordwijk, The Netherlands, 08.-10. Dez. 2010 2010.

[5] Oliver Heirich, Andreas Lehner, Patrick Robertson, and Thomas Strang. Measurement and Analysis of Train Motion and Railway Track Characteristics with Inertial Sensors. In *Intelligent Transportation Systems Conference (ITSC)*, Washington, USA, 2011.

[6] Oliver Heirich, Patrick Robertson, Adrian Cardalda Garcia, and Thomas Strang. Bayesian Train Localization Method Extended By 3D Geometric Railway Track Observations From Inertial Sensors. In *15th International Conference on Information Fusion*, Singapore, 9.-12. Jul. 2012 2012. International Society of Information Fusion (ISIF).

[7] D. V. Hinkley. On the Ratio of Two Correlated Normal Random Variables. *Biometrika*, Vol. 56, No. 3:635–639, 1969.

[8] H. Jochim and F. Lademann. *Planung von Bahnanlagen*. Carl Hanser Verlag München, Germany, 2009.

[9] Bernt Oksendal. *Stochastic Differential Equations Sixth Edition*. Number ISBN 978-3-540-04758-2. Springer, 6 edition, 2007.

BIOGRAPHIES

Boubeker Belabbas is the leader of the Integrity group of the Institute of Communications and Navigation at the German Aerospace Center (DLR) in Oberpfaffenhofen near Munich. He obtained an MSc. degree in Mechanical Engineering from the Ecole Nationale Supérieure de l'Electricité et de Mecanique in Nancy (France) and a specialized Master in Aerospace Mechanics from Ecole Nationale Supérieure de lAéronautique et de l'Espace in Toulouse (France).

In March 2007, Anja Grosch received the German diploma in Computer Engineering from the Ilmenau University of Technology, Germany. After her graduation, she continued working for the communications department in the area of channel coding, OFDM systems and relay networks. Since March 2008, she has been a research associate at the DLR (German Aerospace Center) in the Institute of Communications and Navigation. She joined the integrity group and since then her main focus has been multi-sensor fusion, especially GNSS and INS integration. Furthermore she is developing integrity concepts of these integrated systems optimized for different safety-of-life applications such as civil aviation and railway.

Oliver Heirich graduates in electrical engineering (Dipl.-Ing.) at University of Ulm (Germany) in 2008 and works for the cooperative systems group at DLR. His current research activity involves train localization and railway track mapping based on probabilistic filters with multiple, train-side mounted sensors.

Andreas Lehner was born in Gmunden, Austria. He received the Dipl. Ing. degree in Mechatronics from the University of Linz in 2001 and a Ph.D. in Electrical Engineering from the University Erlangen-Nuremberg in 2007. He is a senior research scientist at the Institute for Communications and Navigation at the German Aerospace Center DLR. His research and project work focuses on safety systems in transportation, the design of vehicle-to-vehicle communication systems, media access control in ad-hoc networks, and on the characterization and analysis of multipath and interference effects in satellite navigation and communication systems.

Thomas Strang is working as a senior researcher in the Institute of Communications and Navigation at the DLR in Oberpfaffenhofen. He joined DLR in 2000 where he is responsible for the Institute's program in transportation research since 2004, which includes new services for Intelligent Transport Systems and adhoc vehicle-to-vehicle communications. Since 2004 he has also been a professor for computer science at the University of Innsbruck. In 2012 he was co-founder of a DLR spin-off company in the ITS domain and since then acting as CEO.